LHC Project Note 121

04 December 1997
Bernard.Jeanneret@cern.ch

Cascade simulations for the betatron cleaning insertion

I. Azhgirey*, I. Baishev*, N. Catalan Lasheras and J.B. Jeanneret

Keywords: radiation, cascade, optics, collimation

Summary

A cascade calculation is done in the IR7 betatron cleaning insertion. It uses a detailed map of the primary losses and an accurate geometrical model of the straight section. One aim is to design a compact shielding which fits in the tight section of the tunnel. The same study allows to define radiation hardness properties of the equipment to be installed in the section and to locate areas of low activity for the installation of sensitive equipment.

1 Introduction

The expected beam losses in collision at LHC shall amount to 8×10^{16} protons per year in the betatron collimation insertion IR7 [1, 2, 3]. This implies the installation of a tight shielding in this area. The primary losses before cascading will be distributed among 20 collimators. The small transverse size of the tunnel imposes to fit the shielding close to the equipments. Cascade calculations must therefore be made with a detailed model of the straight section. In this paper, we report on some preliminary calculations. A first code is used to define a map of primary interactions. Then cascading is made with two versions of the geometry, one with a test version of shielding and one without it. Fluences and doses are computed at the surface of a cylinder surrounding the beam elements. Then, further work to finalise this study is outlined.

2 The betatron cleaning insertion in IR7

2.1 The longitudinal layout of IR7

The collimation system of LHC requires a section of ring which offers a phase advance of $\Delta\mu_x = \Delta\mu_y \approx 2\pi$. This section must not be superconducting to sustain a high level of power deposition [1]. It will be made of six quadrupoles each made of several modules. Two

*Institute for High Energy Physics, Protvino, Russia.
Member of the Russian collaboration to the LHC Project.

bending magnets will be installed at each end of the section to keep the beam line free of the high flux of neutral particles emitted at the primary collimators.

The principles of optics used for a collimation insertion and a discussion of the specific case of the version 5.0 of IR7 in LHC can be found in [3]. The description in [1] was related to the older version 4.2 of the insertion, but the basics of the geometry has not changed.

In this calculation, the primary collimators are made of 200 mm long aluminium jaws and the secondary collimators of 500 mm long copper jaws. These numbers are still open parameters, but are very unlikely to change drastically. The location of the collimators can be found in Section 3.

2.2 The map of primary inelastic collisions

A map of primary inelastic collisions is prepared with the K2 code [3, 4] for further cascade calculations. To get an approximately realistic map of impact on primary collimators , a proton is circulated inside the primary aperture using one turn linear motion superimposed with a variable transverse drift speed until it touches a collimator. Then, a tracking with smaller steps is made, with linear betatronic motion between collimators . In the collimator a Monte-Carlo method is used to simulate coherent and incoherent nuclear elastic and Rutherford scattering. Multiple Coulomb scattering is treated as a continuous diffusion process, iterating the motion near the edge of the collimator with high care. When an inelastic interaction occurs, the tracking is stopped and the coordinates of the proton at the interaction point are stored. The map of inelastic interactions is obtained by tracking ten thousand protons. The small fraction ($< 1\%$) of protons lost at other aperture limitations in the ring are ignored in the present study.

3 Geometrical Model of the Cleaning Section

The cleaning section is described as a sequence of elements aligned in accordance with the optical layout. The elements are primary and secondary collimators, warm dipoles, warm quadrupoles and dipole correctors. Beam pipes in the drift spaces between magnets and collimators are also treated as separate elements.

In the right Cartesian coordinate system (x, y, z) the longitudinal axes of symmetry of dipoles and quadrupoles belongs to the axis z. Beam axes of Ring 1 and Ring 2 lie in parallel to the axis z in the horizontal plane (y, z). The entire chain of elements is fully symmetric with respect to the horizontal plane i.e. has vertical symmetry. At the same time it is horizontally asymmetric because of the location of the orbit correctors and collimators.

Both the extended standard geometry language [5] of the MARS code [6] and several user-written subroutines are used to present the geometry as an ordered set of elementary volumes for the cascade simulations.

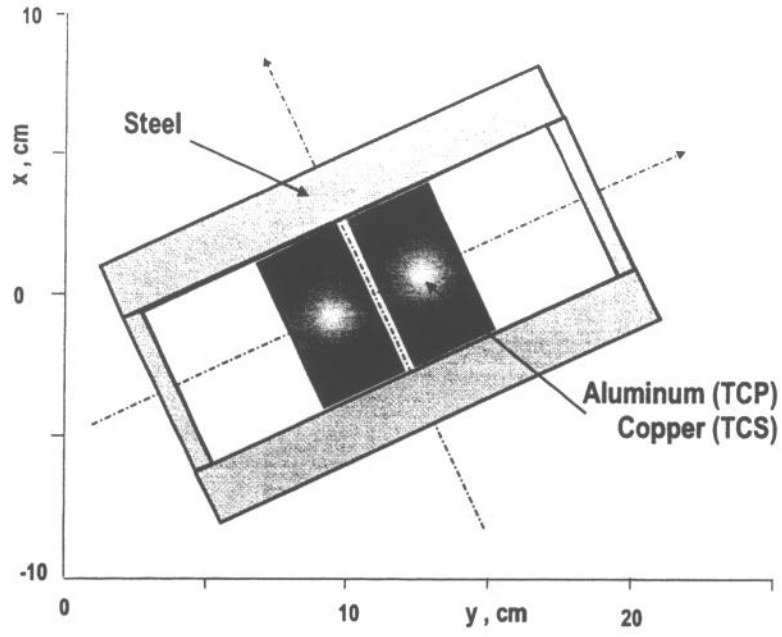

Figure 1: The collimator tank cross-section.

3.1 Elements

Every collimator tank is presented as a pair of jaws in a vacuum box. The longitudinal axis of a collimator coincides with the beam axis of Ring 1 or Ring 2. Both primary (TCP) and secondary (TCS) collimators have the same transverse cross-section but they are different in length and in the jaws material. The cross-section of the collimator tank is shown in Fig.1 for the case of Ring 1 and skew angle of 25 degrees.

The warm dipole and quadrupole modules are described in [7]. The cross-section of the dipole module MBW is shown in Fig.2. The coil material is taken as copper with the effective density 7.4 g/cm^3.

The two-in-one quadrupole module MQW is shown in Fig.3. The two-dimensional maps of the MQW magnetic field calculated by G. De Rijk [8] for both injection and top energy are used to simulate the correct transport of charged particles in the quadrupoles. The warm dipole correctors are placed near every quadrupole in pairs so that the vertical corrector of Ring 1 is accompanied by the horizontal corrector of Ring 2 and vice versa. Every corrector consists of one module MCBW [9]. The transverse cross-section of MCBW is shown in Fig.4 for the case of the horizontal corrector of Ring 1.

Both collimators and magnets are presented for the simulations as sets of elementary straight quadrangular prisms. For example one MQW is described by 134 elementary volumes though only 31 volume satisfactorily describes one MBW.

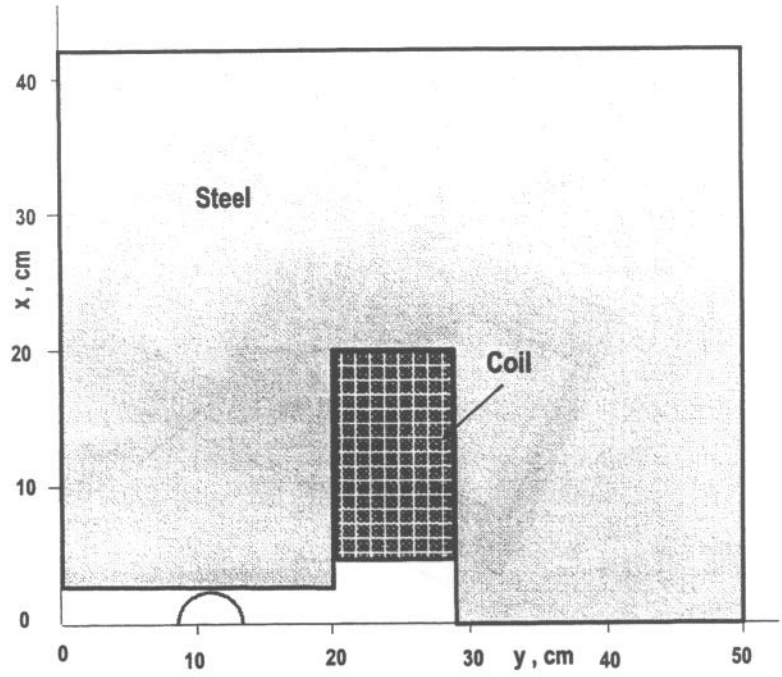

Figure 2: Cross-section of the warm dipole MQW (one quarter).

The beam pipes of both rings are presented as copper tubes. The beam pipe inside magnets and in the short drift spaces between magnets has 44 mm inner diameter and 48 mm outer diameter. These small beam pipes can be seen on the magnet cross-section in Figs.2–4. The inner diameter of the regular beam pipe in the long drift spaces is 100 mm and the outer diameter is 105 mm. These dimensions correspond to the recommendations of the vacuum experts [10].

3.2 Layouts

The initial model of the cleaning section is based on the lattice version 4.2. Fig.6 shows the schematic layout in that case. The more detailed layout with the elements description is given in Table 4. There are three primary collimators in the system: vertical (TCPV), skewed at 45 degrees in the normalized phase space (TCPS) and horizontal (TCPH). Every set of secondary collimators (TCA, TCB and TCC) consists of four units: one horizontal, one vertical and two skewed at 45 and 135 degrees in the normalized phase space. Dipoles D4L and D3L increase the nominal separation between the beams from 194 to 224 mm along the cleaning section. At the end of the section the dipoles D3R and D4R restore the nominal separation.

The total length of the section is 491.9 meters. The total number of the elementary volumes in the model 4.2 is equal to 3810.

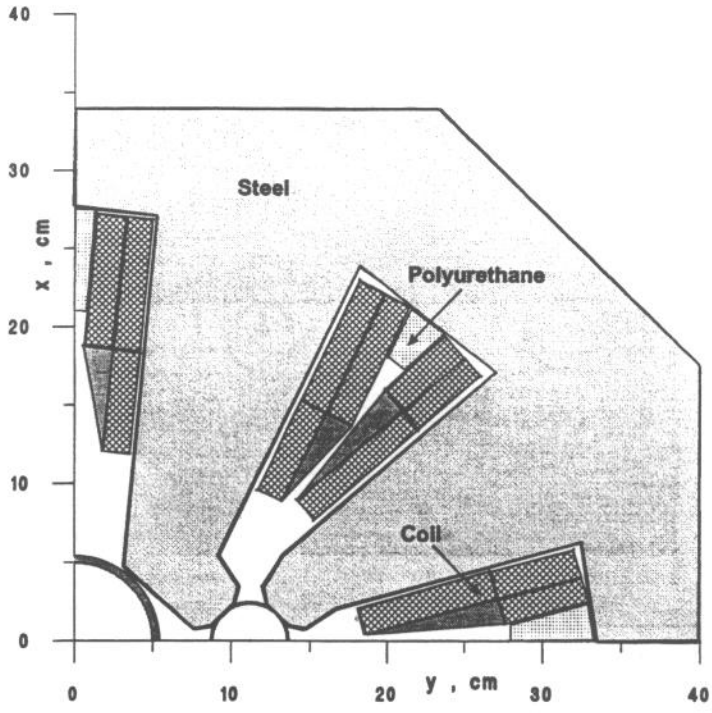

Figure 3: Cross-section of the warm quadrupole MQW (one quarter).

The continuous work [11] on the optimization of the beam cleaning system resulted in the lattice version 5.0. The latest model of the cleaning section is shown schematically in Fig.7 and described in more details in Table 5. Four primary collimators are : vertical (TCPV1), 45 degrees skew (TCPS1), 135 degrees skew (TCPS2) and horizontal (TCPH1). Each of secondary collimators (TCS01–TCS16) has an individual position and an individual skew.

The total length of the section is 502 meters. The total number of the elementary volumes in the model 5.0 is equal to 5546.

3.3 Optional Shielding

Reasonable maximum of material around the beam lines is the first approach to the shielding design of the cleaning system. Iron shielding covers all the drifts between magnets. Transverse cross-section of the shielding is shown in Fig.5. The outer dimensions of the shielding are approximately the same as the outer dimensions of the dipoles. The inner dimensions h_s and v_s are determined by the minimum space required for the beam pipes or collimators (see Table 1). The shielding is described in the model 5.0 by 172 elementary volumes.

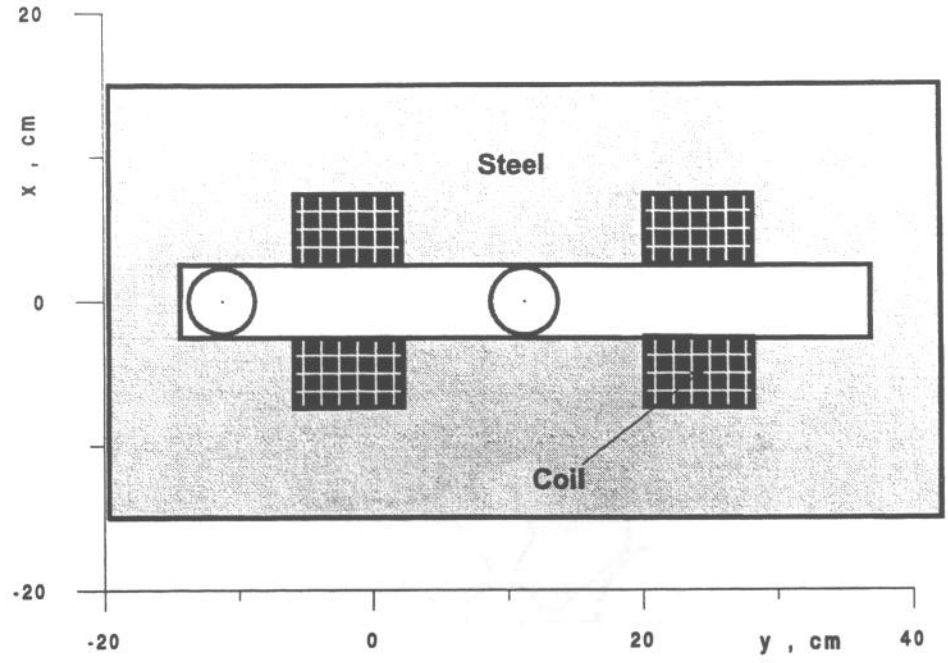

Figure 4: Cross-section of the dipole corrector MCBW in the horizontal position.

Table 1: Inner dimensions of the shielding around collimators and drifts.

Size, [cm]	Collimators	105 mm beam pipe	48 mm beam pipe
h_s	50	34	30
v_s	26	12	6

3.4 Scoring Shell

Thin (1 cm) cylindrical vacuum layer surrounding the whole assembly of elements is used for scoring the rate of outgoing particles. The shell is subdivided both azimuthally as shown in Fig.5 and longitudinally with 1 metre step. The azimuthal subdivisions named L, R and UD arcs reflect the horizontal asymmetry and vertical symmetry of the system. The total number of the scoring cells is equal to 1474 and to 1506 in the models 4.2 and 5.0 respectively. To compute doses, the same cylinder layer is filled with polystyrene in a separate calculation made for version 5.0.

3.5 Optical Test

Both models 4.2 and 5.0 are tested from the optical point of view in order to avoid any error in longitudinal and transverse positions of the elements. The test beam is simulated as a circumference of radius n in the normalized coordinate system using Twiss parameters

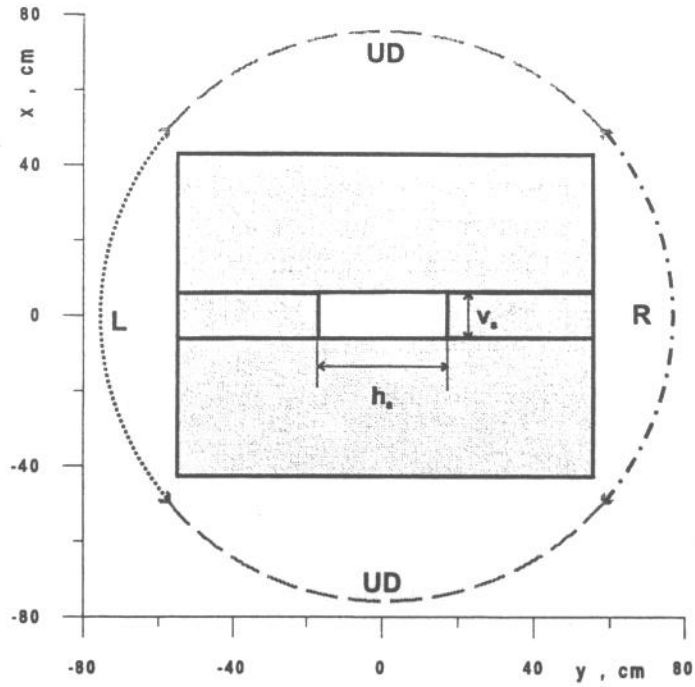

Figure 5: Cross-section of the shielding and scoring shell.

for the coordinates conversion to the reference system. The primary collimators ($n = 6$) are tested first with $n = 5.95$ and after that the secondary collimators ($n = 7$) are tested with $n = 6.95$ and with retracted primary ones. When all the test beam particles come out successfully the test is repeated with the beam of slightly larger radius $n = 6.05$ and $n = 7.05$ correspondingly. In that case all or almost all the particles are registered by the collimators.

4 Results

Hadronic and electromagnetic cascades simulations were performed with the last version of the MARS code. Energy cut-off for hadron transport is 10 MeV.

The longitudinal distribution of hadron fluence in the scoring shell are presented in Figs.8–17. Similar distributions of the absorbed dose in the thin organic filler of the scoring shell are presented in Figs.19–22. Each figure is supplied with the corresponding geometry scheme where the shielding is shown when necessary.

4.1 Model 4.2

The model 4.2 is somewhat obsolete but it is simpler than the model 5.0 and the results for the former have basically the introductory purpose. Fig.8 shows how the superposition

of fluences generated by the opposing beams results in the quasi-symmetric longitudinal distribution. The full symmetry about the interaction point is reached in the UD case only (see Fig.9c). The longitudinal distributions for UD, R and L scoring arcs shown in Fig.9a,b are similar but the difference between them can be seen clearly.

The structure of the single-beam distributions reflects both the map of primary interactions and the spread of high energy secondaries along the beamline. Three well-separated major peaks downstream of the secondary collimator locations can be explained by both the complete development of the cascades in their thick jaws and the interception of high energy secondaries from upstream collimators.

4.2 Model 5.0

The longitudinal distributions for the model 5.0 are obviously different from those for the model 4.2 due to significant changes in the collimator longitudinal positions. The set of moderate peaks around TCS03–TCS16 in Fig.10 replaces two prominent peaks around TCB and TCC in Fig.8. The better longitudinal resolution of Figs.11–14 lets one to assign each peak to the certain collimator.

At injection (see Fig.15) the longitudinal distribution of the hadron fluence is almost the same as at collisions except in the dogleg region. It can be seen more clearly in Figs.16, 17 along with the fact that the yearly contribution of injection to fluences is noticeable but not significant. The annual values are obtained under assumption of 10^{16} and 1.6×10^{16} inelastic interactions of halo protons in collimators of one ring per year for injection and collisions [2] respectively.

Table 2 gives the summary of longitudinally averaged values indicating lateral leakage of hadrons from the cleaning section for the model 5.0.

Table 2: Average fluence $< F >$ of hadrons, their total energy E_s, average current I_t and average energy of one hadron $< E >$ at collisions without/with shielding (Col/Col Sh) and at injection (Inj/Inj Sh).

Setup	$< F(L) >$ $h/cm^2/p$	$< F(R) >$ $h/cm^2/p$	$< F(UD) >$ $h/cm^2/p$	$< F >$ $h/cm^2/p$	E_s GeV	I_t $hadrons$	$< E >$ MeV
Col	1.73-4	2.89-4	2.11-4	2.20-4	802	2100	380
Col Sh	5.90-5	1.19-4	4.94-5	6.68-5	125	1140	110
Inj	2.15-5	3.41-5	2.77-5	2.77-5	93	270	350
Inj Sh	6.97-6	1.38-5	5.66-6	7.74-6	14.5	130	110

4.3 Shielding Effect

Study of the shielding effect is the main goal of these calculations with the model 5.0. Fluence attenuation by the shielding varies from factor 1 to factor 30 and is the higher the longer is the distance from the closest source of radiation as can be seen in Figs.10–14. The shielding effect depends on both kind and energy of hadrons as shown in Fig.18.

Hadron fluence is a good indicator with respect to the radioactivation of the machine components, cooling water, air in the tunnel and rock outside. Dose is the better indicator with respect to the radiation damage of cable organic insulation and other organic parts of equipment. Shielding effect in the case of absorbed dose is significantly stronger than in the case of hadron fluence as can be seen in Figs.19–22, where each unshielded short drift between magnet modules is marked by a peak in longitudinal distribution. It is explained by much better attenuation of electrons and photons in the material in comparison with hadron attenuation.

The integral shielding efficiencies defined by the ratio of values $< F >$, I_t, E_s and the longitudinally averaged absorbed dose D_a in the case without shielding to the same values in the case with shielding are presented in Table 3.

Table 3: Integral shielding efficiency in terms of hadron fluence $< F >$ and current I_t, total energy of hadrons E_s and annual absorbed dose D_a.

Value	L	UD	R	averaged
$< F >$, collisions	2.9	4.3	2.4	3.3
$< F >$, injection	3.1	4.9	2.5	3.6
I_t, collisions				1.8
E_s, collisions				6.4
E_s, injection				8.6
D_a	29	50	23	35

5 Summary and Further Tasks

The described first stage of the radiation studies for the LHC cleaning insertions includes:

- simulation of the cleaning process resulting in the complete determination of the primary source of radiation;
- creation and development of the geometrical model of the cleaning section for cascade simulations;
- nuclear and electromagnetic cascade simulations resulting in the detailed data on the radiation levels around the beam cleaning system;
- the estimation of the effect of the shielding.

In agreement with G. Stevenson the next step of the studies foresees the estimation of the residual radiation levels in the tunnel and calculation of the air and cooling water activation. Study of dose distribution in the magnet coils is the following task.

6 Acknowledgements

The authors of this note would like to thank G.R. Stevenson for his help in the formulation of the problem and numeral discussions of the shielding design. The authors are grateful to W. Middelkoop, T. Taylor and K. Potter for their constant support of this work, and to M. Giesch and G. De Rijk for the introduction to the warm magnet design and magnetic field map calculations.

References

[1] *"The large hadron collider, Conceptual design"*, The LHC study group, CERN/AC/95-05 (LHC), October 1996.

[2] M.Hofert, K.Potter and G.R.Stevenson, *"Summary of Design Values, Dose Limits, Interaction Rates etc. for use in estimating Radiological Quantities associated with LHC Operation"*, CERN/TIS-RP/IR/95-19.1 (1995).

[3] N. Catalan Lasheras, G. Ferioli, J.B. Jeanneret et al., *"Proton Collimation in TeV Colliders"*, LHC Report 156, October 1997.

[4] T.Trenkler and J.B. Jeanneret, CERN SL/Note 94-105 (AP), 1994.

[5] V.V.Talanov, *"Universal Geometrical Module for MARS Program"*, Preprint IHEP 92-99, Protvino, 1992 (in russian).

[6] I.L.Azhgirey, I.A.Kurochkin and V.V.Talanov, *"MARS program complex development for radiation aspects of electro-nuclear devices design"*, in: Annotations of XV Workshop on Charged Particles Accelerators, p.74, Protvino, 22-24.10.96 (in russian).

[7] M. Giesch, *"Design and Parameters of the Warm Magnets for the LHC Cleaning Insertions"*, CERN AT/95-04, LHC Note 311, 1995; M. Giesch, LHC Note 323, November 1995.

[8] G. De Rijk, LHC Project Note 100, August 1997.

[9] G. De Rijk, to appear at EPAC 98, 1998.

[10] A.G.Mathewson and S.Zhang, *"The LHC Warm Straights Vacuum System"*, CERN AT-VA/AGM 95-23 (1995).

[11] D.I.Kaltchev, M.K.Craddock, R.V.Servranckx and J.B.Jeanneret, *"Numerical Optimization of Collimator Jaw Orientations and Locations in the LHC"*, in PAC 97, Vancouver, June 1997 and CERN LHC Proj. Rep. 134, 1997.

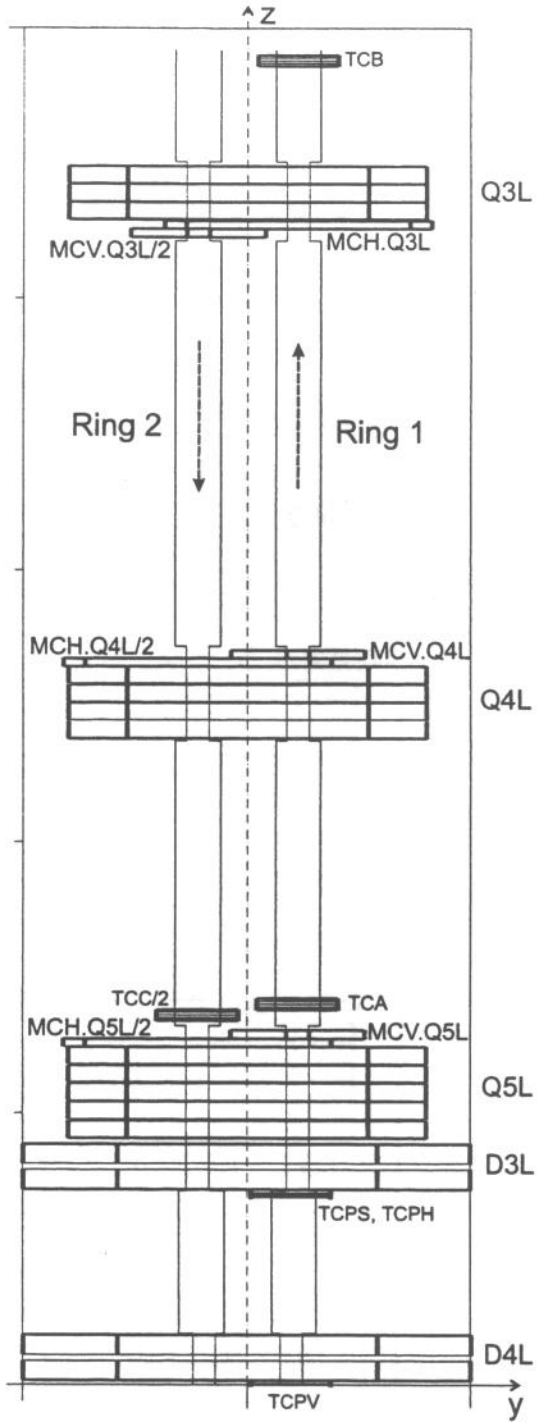

Figure 6: Layout of the left part of the cleaning insertion (lattice version 4.2).

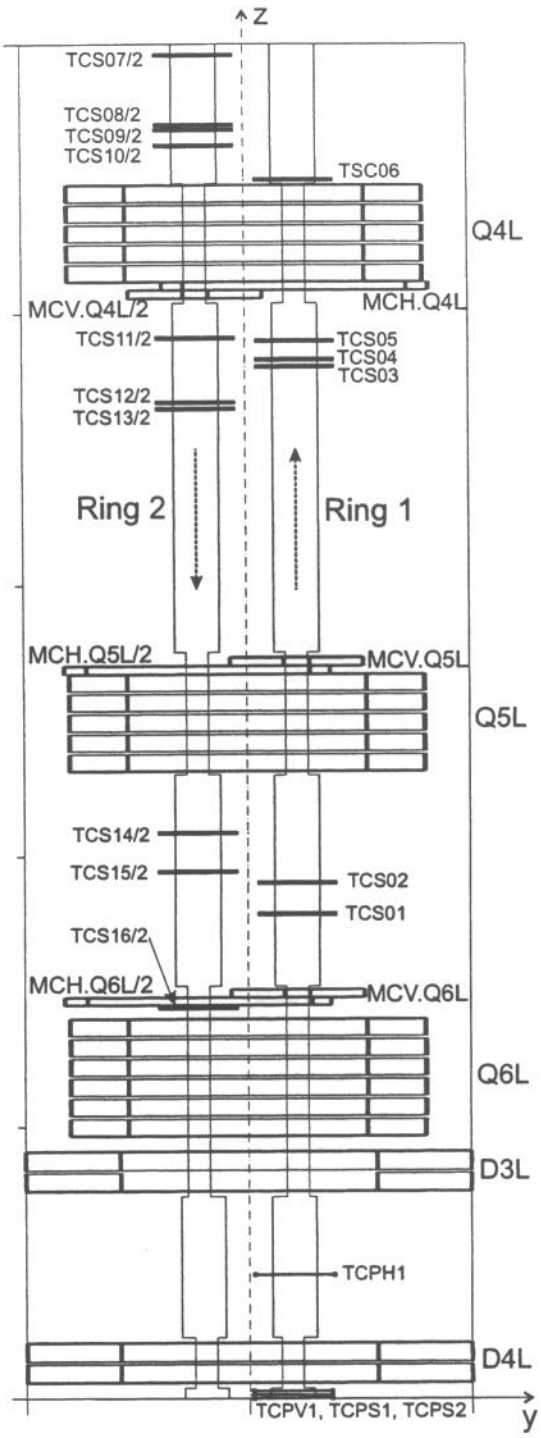

Figure 7: Layout of the left part of the cleaning insertion (lattice version 5.0).

Table 4: Elements of the cleaning insertion (lattice version 4.2)

Name	Entrance [m]	Length [m]	Element description, quantity and type of modules
TCPV	0.00	0.2	Primary collimator vertical, 1 TCP
D4L	0.80	7.5	Warm separation dipole, 2 MBW
TCPS	34.65	0.2	Primary collimator skewed, 1 TCP
TCPH	35.25	0.2	Primary collimator horizontal, 1 TCP
D3L	36.05	7.5	Warm separation dipole, 2 MBW
Q5L	45.45	16.7	Warm quadrupole, 5 MQW
MCH.Q5L/2	62.15	1.5	Dipole corrector horizontal of Ring 2, 1 MCBW
MCV.Q5L	63.65	1.5	Dipole corrector vertical, 1 MCBW
TCC/2	65.15	2.0	Secondary collimator of Ring 2, 4 TCS
TCA	67.15	2.0	Secondary collimator, 4 TCS
Q4L	119.00	13.3	Warm quadrupole, 4 MQW
MCH.Q4L/2	132.30	1.5	Dipole corrector horizontal of Ring 2, 2 MCBW
MCV.Q4L	133.80	1.5	Dipole corrector vertical, 1 MCBW
MCV.Q3L/2	211.25	1.5	Dipole corrector vertical of Ring 2, 1 MCBW
MCH.Q3L	212.75	1.5	Dipole corrector horizontal, 1 MCBW
Q3L	214.45	9.9	Warm quadrupole, 3 MQW
TCB	243.95	2.0	Secondary collimator, 4 TCS
IP3	245.95	0.0	Marker
TCB/2	245.95	2.0	Secondary collimator of Ring 2, 1 TCS
Q3R	267.55	9.9	Warm quadrupole, 3 MQW
MCH.Q3R/2	277.65	1.5	Dipole corrector horizontal of Ring 2, 1 MCBW
MCV.Q3R	279.15	1.5	Dipole corrector vertical, 1 MCBW
MCV.Q4R/2	356.60	1.5	Dipole corrector vertical of Ring 2, 1 MCBW
MCH.Q4R	358.10	1.5	Dipole corrector horizontal, 1 MCBW
Q4R	359.60	13.3	Warm quadrupole, 4 MQW
TCA/2	422.75	2.0	Secondary collimator of Ring 2, 4 TCS
TCC	424.75	2.0	Secondary collimator, 4 TCS
MCV.Q5R/2	426.75	1.5	Dipole corrector vertical of Ring 2, 1 MCBW
MCH.Q5R	428.25	1.5	Dipole corrector horizontal, 1 MCBW
Q5R	429.75	16.7	Warm quadrupole, 5 MQW
D3R	448.35	7.5	Warm separation dipole, 2 MBW
TCPH/2	456.65	0.2	Primary collimator horizontal of Ring 2, 1 TCP
TCPS/2	457.45	0.2	Primary collimator skewed of Ring 2, 1 TCP
D4R	483.60	7.5	Warm separation dipole, 2 MBW
TCPV/2	491.70	0.2	Primary collimator vertical of Ring 2, 1 TCP

Table 5: Elements of the cleaning insertion (lattice version 5.0)

Name	Entrance [m]	Length [m]	Element description, quantity and type of modules
TCPV1	0.066	0.2	Primary collimator vertical, 1 TCP
TCPS1	0.576	0.2	Primary collimator skewed, 1 TCP
TCPS2	1.340	0.2	Primary collimator skewed, 1 TCP
D4L	2.925	7.3	Warm separation dipole, 2 MBW
TCPH1	22.842	0.2	Primary collimator horizontal, 1 TCP
D3L	38.190	7.3	Warm separation dipole, 2 MBW
Q6L	48.340	21.6	Warm quadrupole, 6 MQW
TCS16/2	71.959	0.5	Secondary collimator of Ring 2, 1 TCS
MCH.Q6L/2	72.459	1.5	Dipole corrector horizontal of Ring 2, 1 MCBW
MCV.Q6L	73.959	1.5	Dipole corrector vertical, 1 MCBW
TCS01	89.369	0.5	Secondary collimator, 1 TCS
TCS02	95.104	0.5	Secondary collimator, 1 TCS
TCS15/2	97.164	0.5	Secondary collimator of Ring 2, 1 TCS
TCS14/2	104.288	0.5	Secondary collimator of Ring 2, 1 TCS
Q5L	115.693	17.9	Warm quadrupole, 5 MQW
MCH.Q5L/2	133.693	1.5	Dipole corrector horizontal of Ring 2, 1 MCBW
MCV.Q5L	135.193	1.5	Dipole corrector vertical, 1 MCBW
TCS13/2	182.400	0.5	Secondary collimator of Ring 2, 1 TCS
TCS12/2	183.648	0.5	Secondary collimator of Ring 2, 1 TCS
TCS03	190.254	0.5	Secondary collimator, 1 TCS
TCS04	191.519	0.5	Secondary collimator, 1 TCS
TCS05	195.040	0.5	Secondary collimator, 1 TCS
TCS11/2	195.540	0.5	Secondary collimator of Ring 2, 1 TCS
MCV.Q4L/2	202.881	0.5	Dipole corrector vertical of ring 2, 1 MCBW
MCH.Q4L	204.381	1.5	Dipole corrector horizontal, 1 MCBW
Q4L	205.981	17.9	Warm quadrupole, 5 MQW
TCS06	224.875	0.5	Secondary collimator, 1 TCS
TCS10/2	231.216	0.5	Secondary collimator of Ring 2, 1 TCS
TCS09/2	234.216	0.5	Secondary collimator of Ring 2, 1 TCS
TCS08/2	235.028	0.5	Secondary collimator of Ring 2, 1 TCS
TCS07/2	247.960	0.5	Secondary collimator of Ring 2, 1 TCS
IP7	251.000	0.0	Marker
TCS07	253.540	0.5	Secondary collimator, 1 TCS
TCS08	266.472	0.5	Secondary collimator, 1 TCS
TCS09	267.284	0.5	Secondary collimator, 1 TCS
TCS10	270.284	0.5	Secondary collimator, 1 TCS

Table 5 continuation.

Name	Entrance [m]	Length [m]	Element description, quantity and type of modules
TCS06/2	276.625	0.5	Secondary collimator of Ring2, 1 TCS
Q4R	278.119	17.9	Warm quadrupole, 5 MQW
MCH.Q4R/2	296.119	1.5	Dipole corrector horizontal of Ring 2, 1 MCBW
MCV.Q4R	297.619	1.5	Dipole corrector vertical, 1 MCBW
TCS11	305.960	0.5	Secondary collimator, 1 TCS
TCS05/2	306.460	0.5	Secondary collimator of Ring 2, 1 TCS
TCS04/2	309.981	0.5	Secondary collimator of Ring 2, 1 TCS
TCS03/2	311.246	0.5	Secondary collimator of Ring 2, 1 TCS
TCS12	317.852	0.5	Secondary collimator, 1 TCS
TCS13	319.100	0.5	Secondary collimator, 1 TCS
MCV.Q5R/2	365.307	1.5	Dipole corrector vertical of Ring 2, 1 MCBW
MCH.Q5R	366.807	1.5	Dipole corrector horizontal, 1 MCBW
Q5R	368.407	17.9	Warm quadrupole, 5 MQW
TCS14	397.212	0.5	Secondary collimator, 1 TCS
TCS15	404.336	0.5	Secondary collimator, 1 TCS
TCS02/2	406.396	0.5	Secondary collimator of Ring 2, 1 TCS
TCS01/2	412.131	0.5	Secondary collimator of Ring 2, 1 TCS
MCV.Q6R/2	426.541	1.5	Dipole corrector vertical of Ring2, 1 MCBW
MCH.Q6R	428.041	1.5	Dipole corrector horizontal, 1 MCBW
TCS16	429.541	0.5	Secondary collimator, 1 TCS
Q6R	435.760	21.6	Warm quadrupole, 6 MQW
D3R	456.510	7.3	Warm separation dipole, 2 MBW
TCPH1/2	478.958	0.2	Primary collimator of Ring 2, 1 TCP
D4R	491.775	7.3	Warm separation dipole, 2 MBW
TCPS2/2	500.460	0.2	Primary collimator of Ring 2, 1 TCP
TCPS1/2	501.224	0.2	Primary collimator of Ring 2, 1 TCP
TCPV1/2	501.734	0.2	Primary collimator of Ring 2, 1 TCP

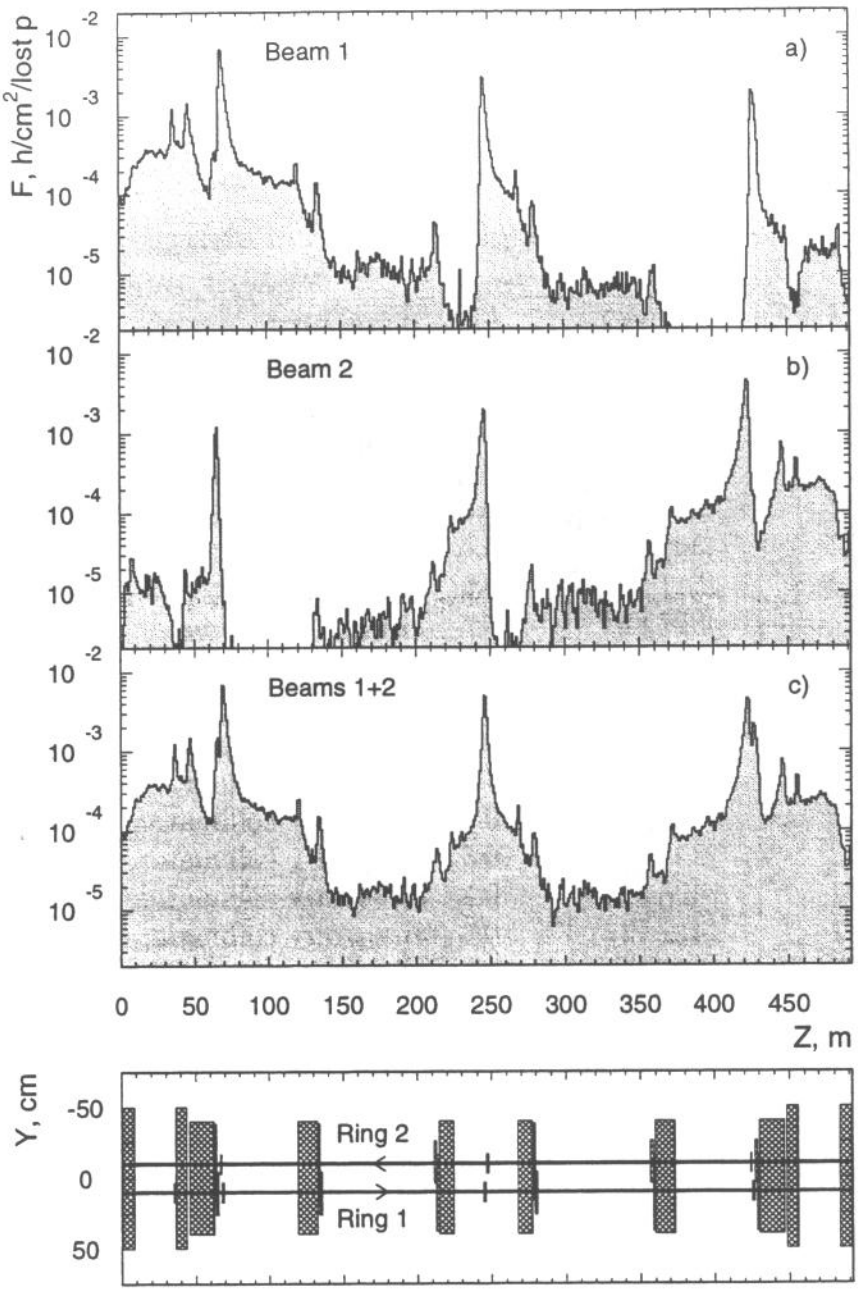

Figure 8: Fluence of hadrons around the cleaning system (lattice version 4.2) in the scoring arc L: (a) – generated by the first beam; (b) – generated by the second beam; (c) – superposition of both beams contributions. Fluence is normalized per one interacting proton of one beam.

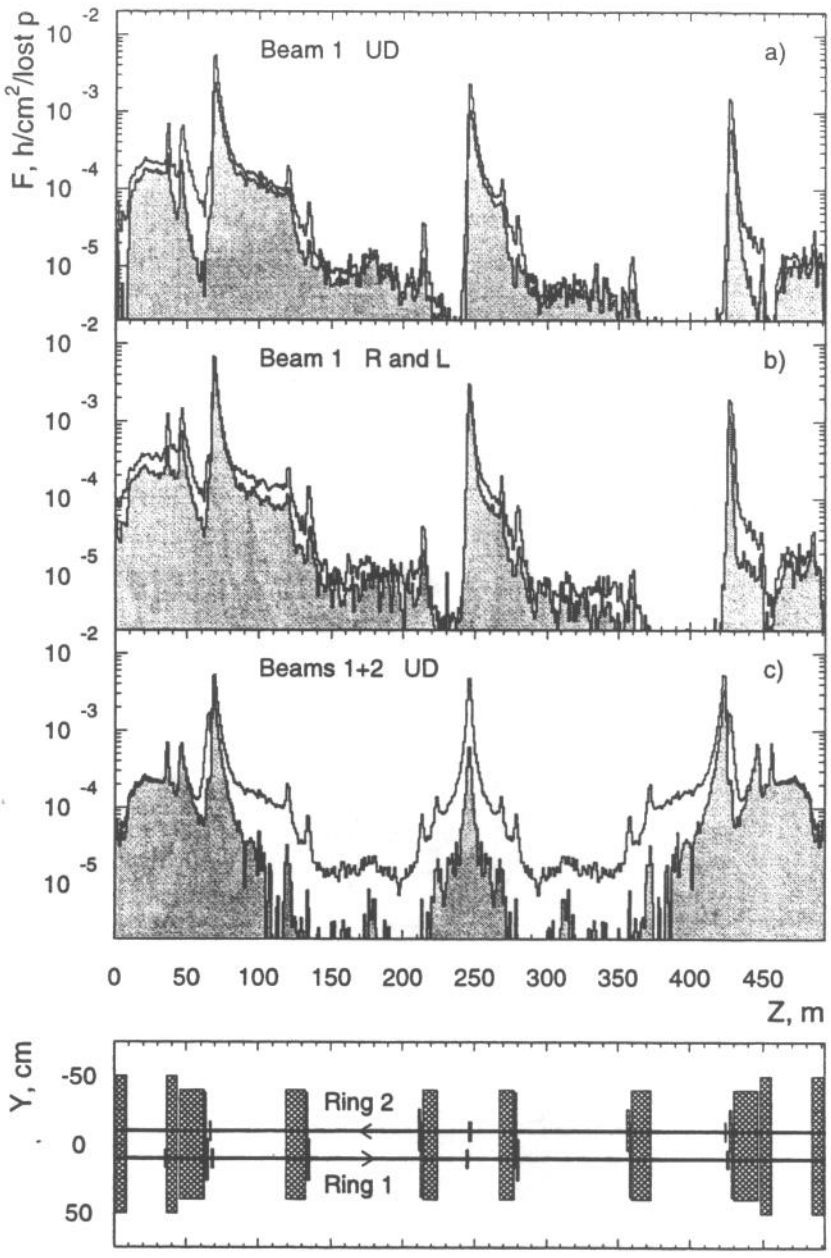

Figure 9: Fluence of hadrons around the cleaning system (lattice version 4.2): (a) – generated by the first beam in UD scoring arcs, clear histogram – all hadrons, grey – charged ones; (b) – generated by the first beam in scoring arc R (clear histogram) and L (grey histogram); (c) – generated by both beams in UD scoring arcs, the grey histogram is for the hypothetical case of absence of any primary interaction in the secondary collimators. Fluence is normalized per one interacting proton of one beam.

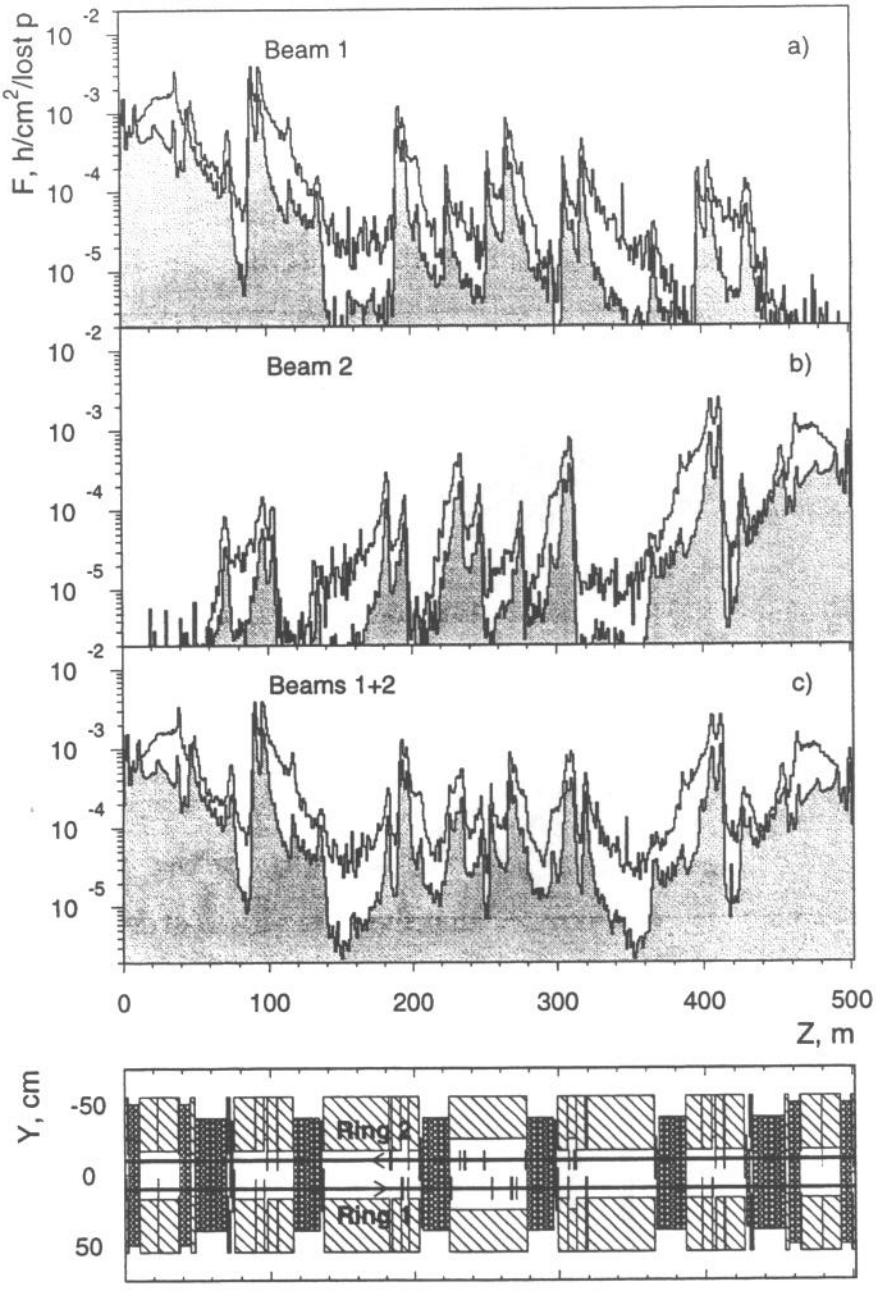

Figure 10: Fluence of hadrons around the cleaning system (lattice version 5.0) in scoring arc L: (a) – generated by the first beam; (b) – generated by the second beam (b); (c) – superposition of both beams contributions. Clear histograms - the case without shielding, grey histograms - the case with shielding. Fluence is normalized per one interacting proton of one beam.

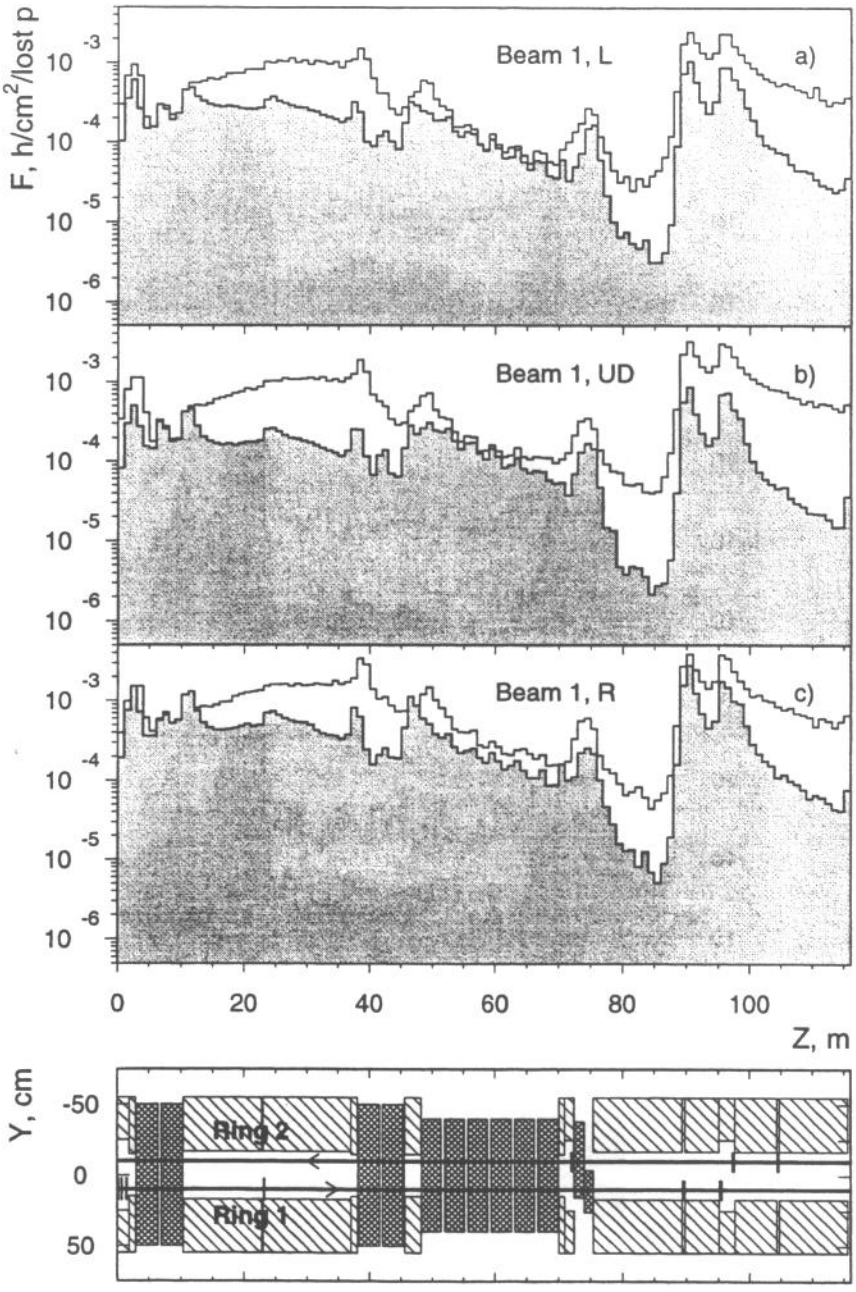

Figure 11: The same as Fig.11 for the dogleg and Q6L regions.

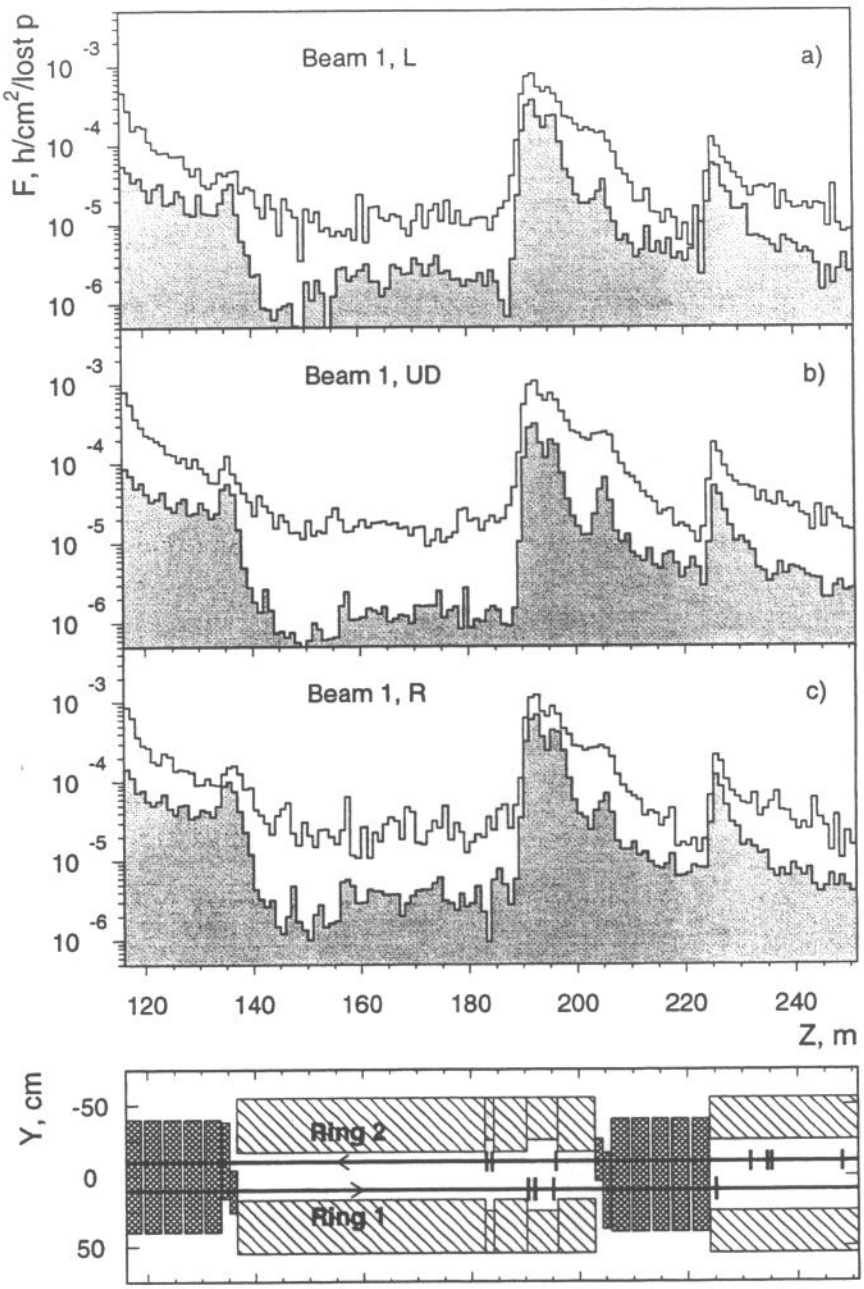

Figure 12: The same as Fig.11 for Q5L and Q4L regions.

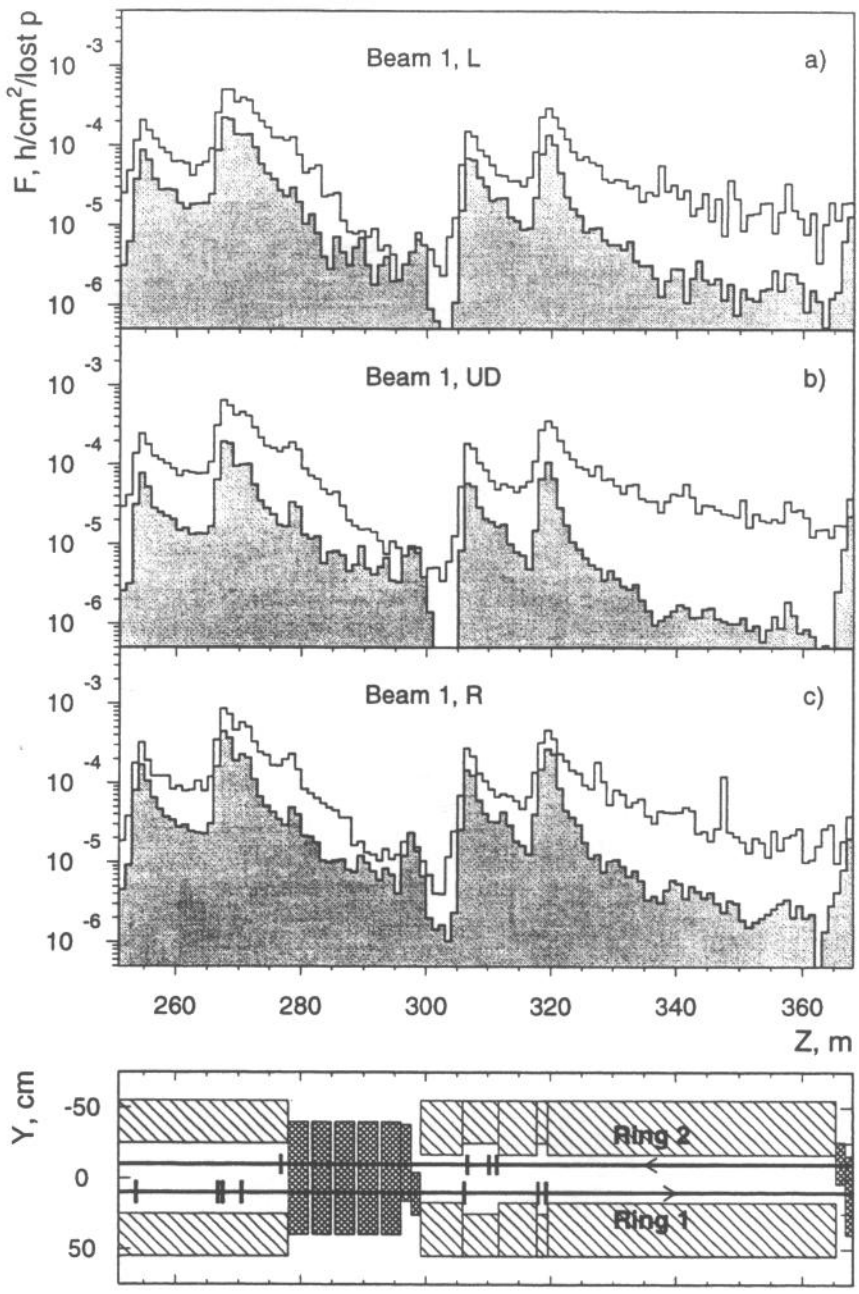

Figure 13: The same as Fig.11 for Q4R region.

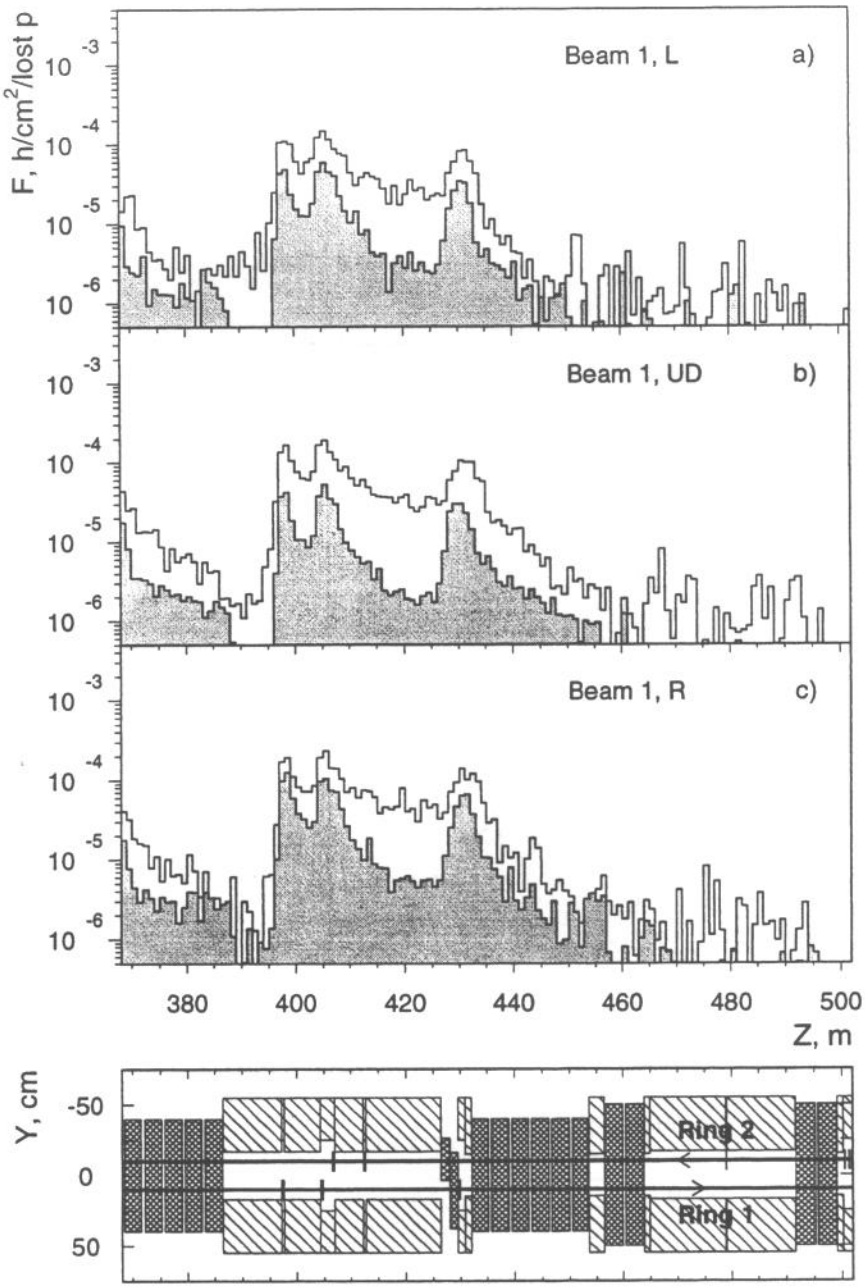

Figure 14: The same as Fig.11 for Q5R, Q6R and dogleg regions.

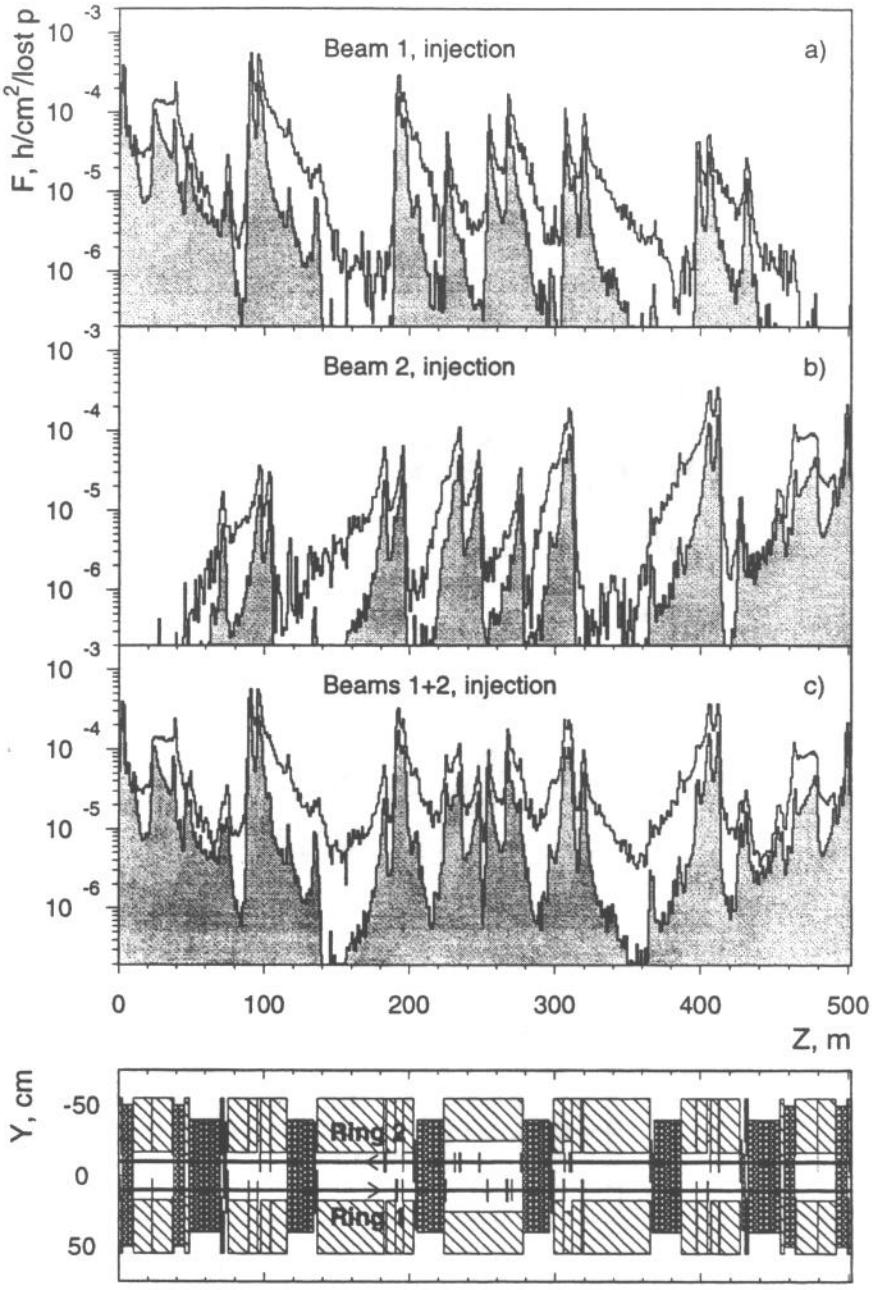

Figure 15: The same as Fig.11 for injection energy.

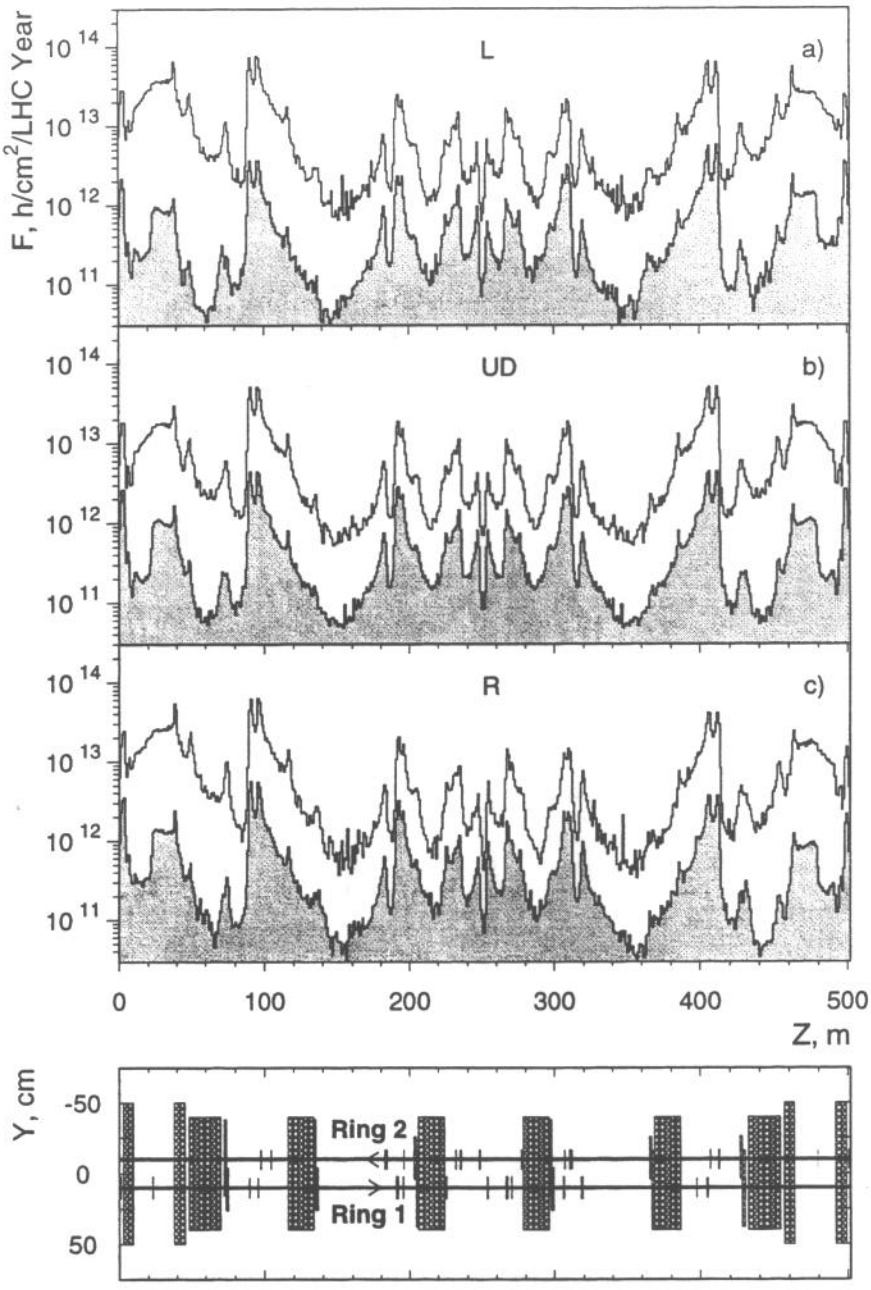

Figure 16: Annual fluences around the cleaning system in the case without shielding: (a) – in the scoring arc L; (b) – in the scoring arcs UD; (c) – in the scoring arc R. Clear histograms are for collisions energy, grey histograms - for injection energy.

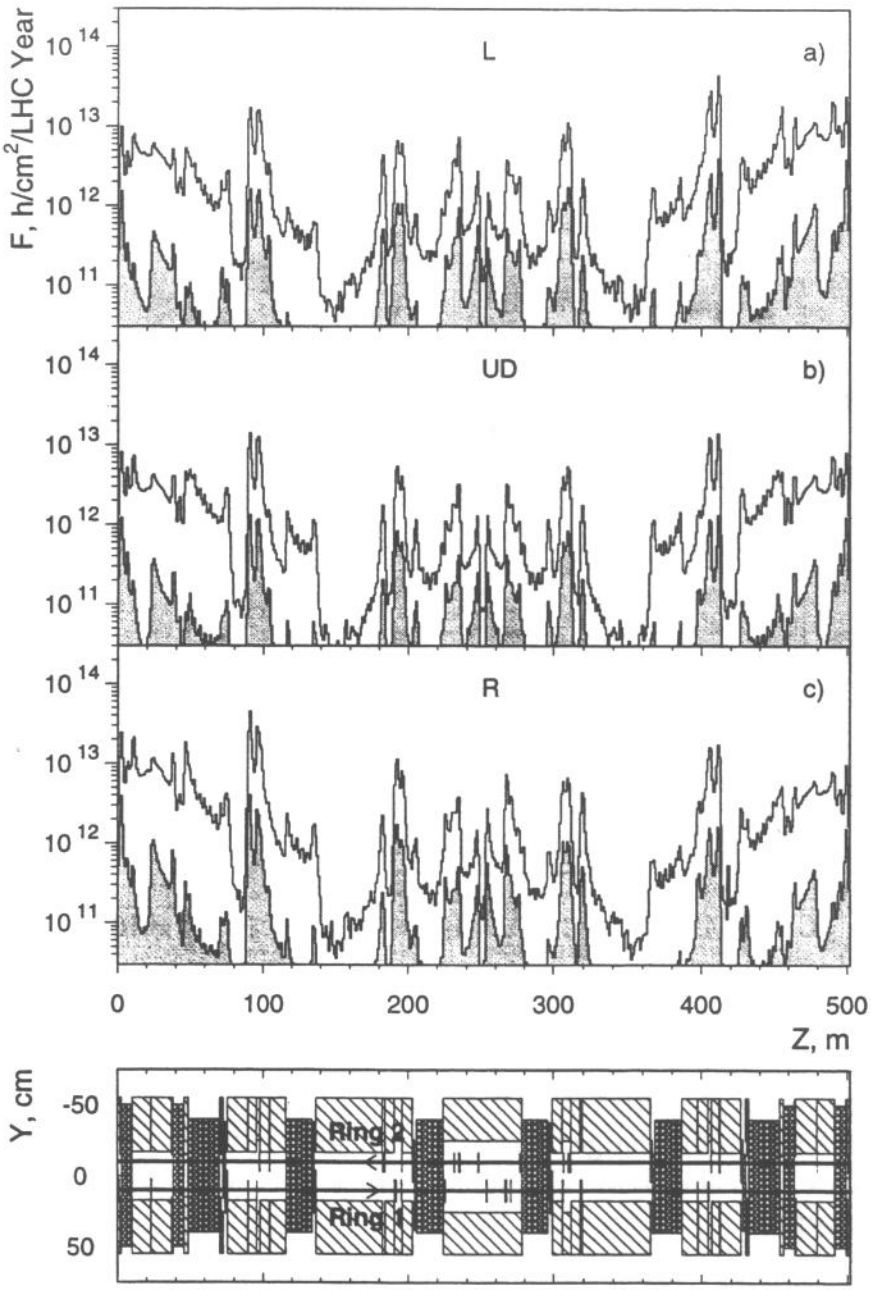

Figure 17: The same as Fig.17 in the case with shielding.

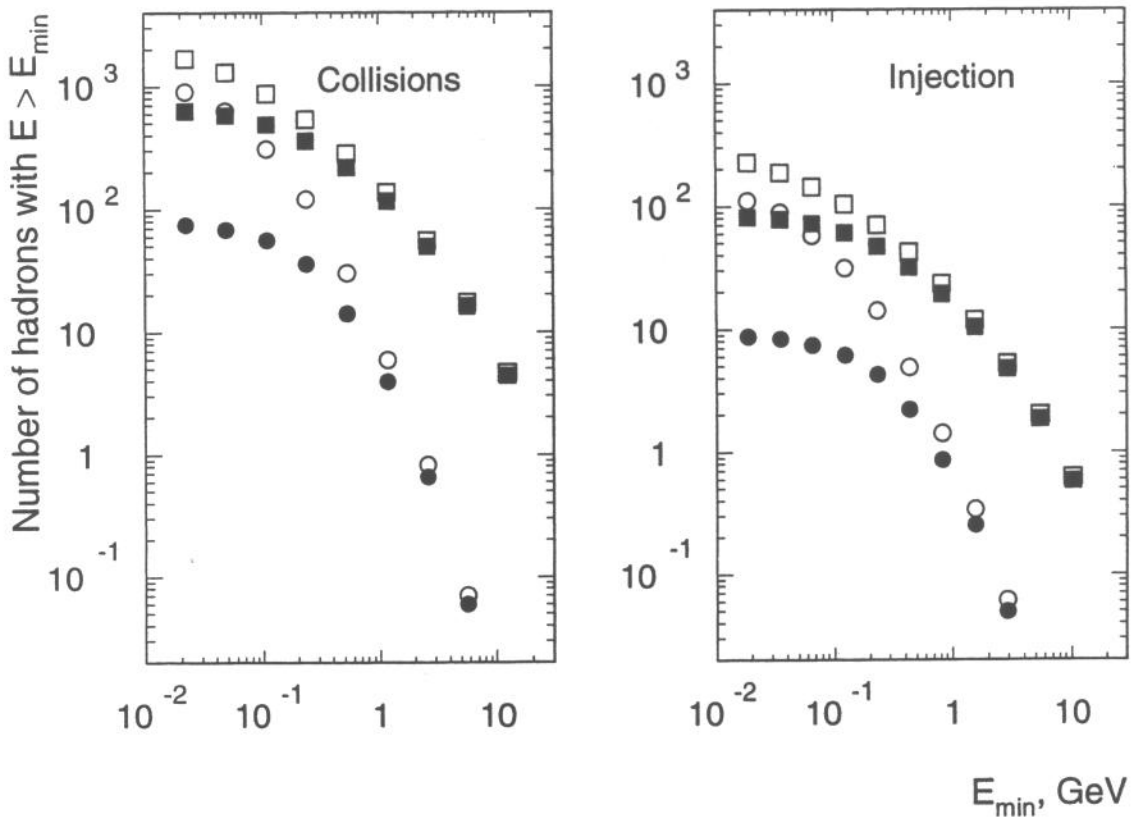

Figure 18: Integral spectra of hadrons in the scoring shell. Clear symbols are for all hadrons, solid symbols are for charged ones. Squares are for the case without shielding and circles - for the case with shielding. The number of hadrons is normalized per one interacting proton of one beam.

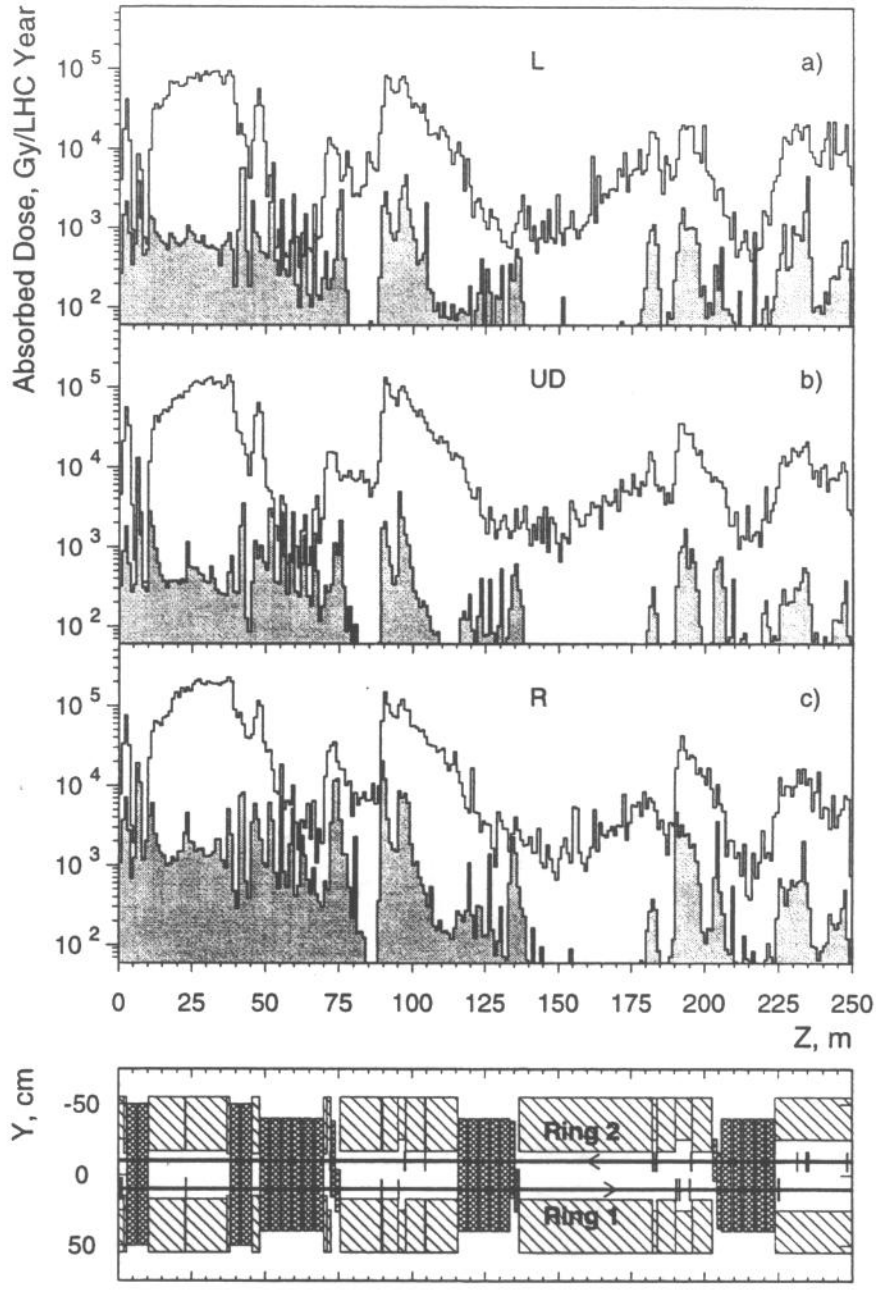

Figure 19: Annual absorbed dose in organic material around the cleaning section: (a) – in the scoring arc L; (b) – in the scoring arcs UD; (c) – in the scoring arc R. Clear histograms - the case without shielding, grey - the case with shielding.

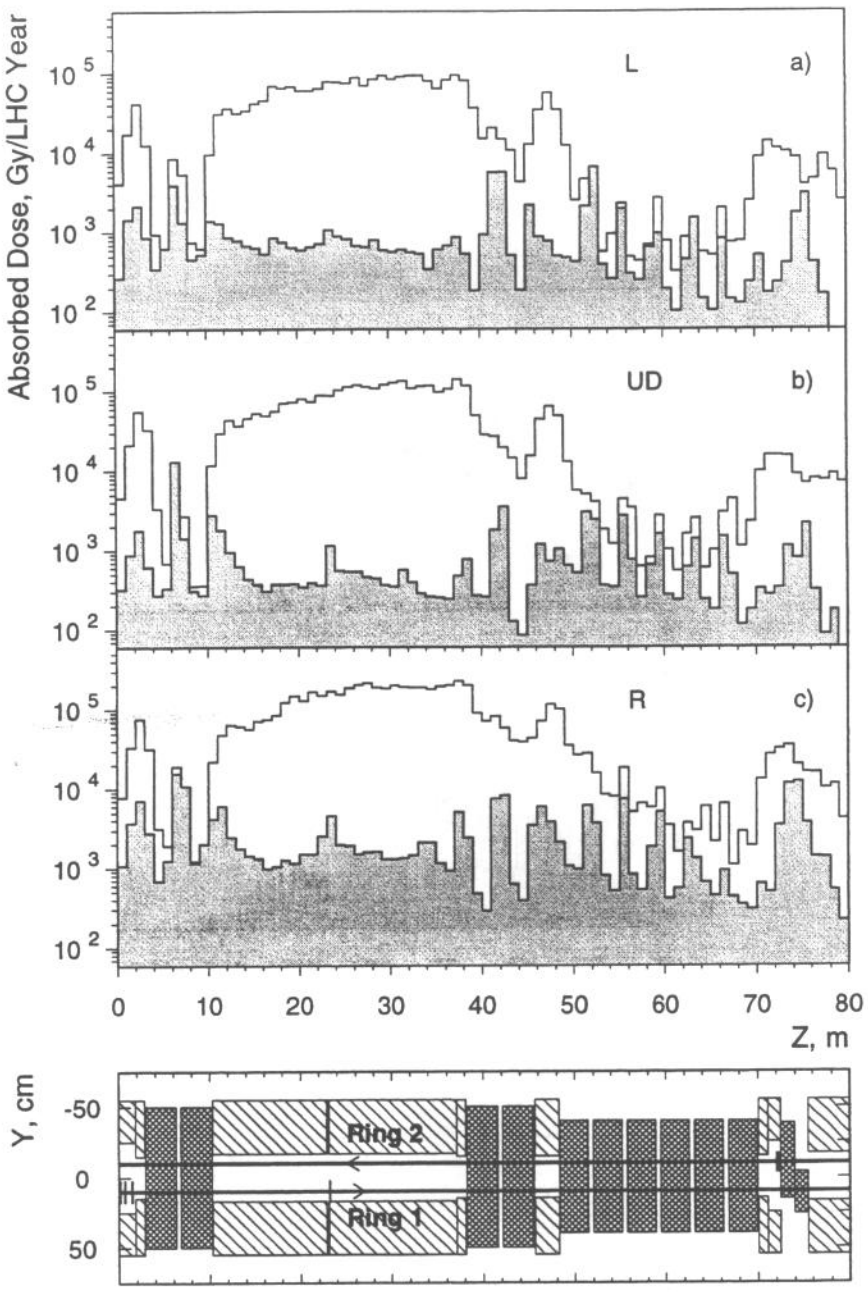

Figure 20: The same as Fig.20 for the dogleg and Q6L regions.

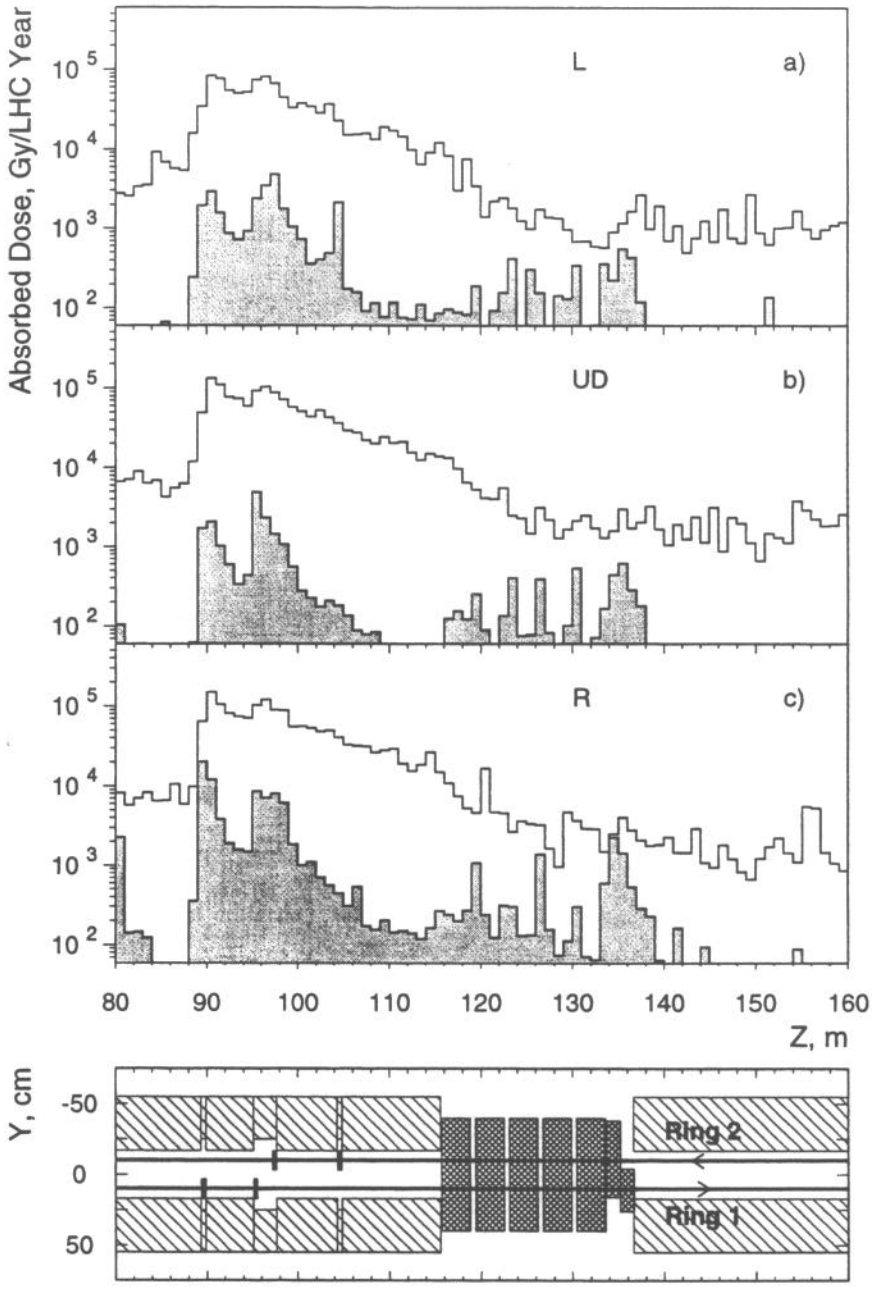

Figure 21: The same as Fig.20 for Q5L region.

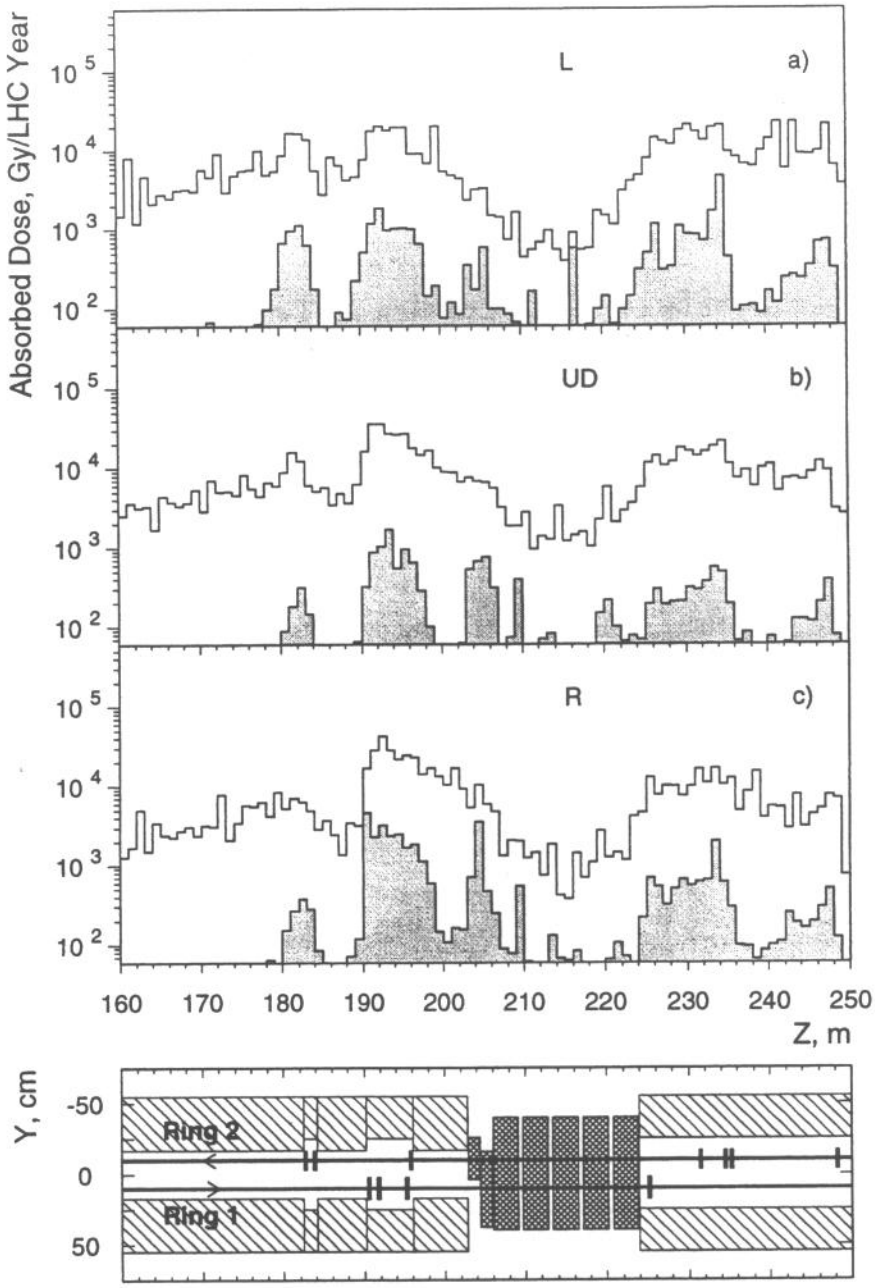

Figure 22: The same as Fig.20 for Q4L region.